

Vibronic activation of molecular vibrational overtones in the infrared spectra of charge-ordered organic conductors

Kaoru Yamamoto,* Aneta Aniela Kowalska, Yue Yue, and Kyuya Yakushi

Institute for Molecular Science, Myodaiji, Okazaki, Aichi 444-8585, Japan

(Received 18 October 2010; revised manuscript received 23 March 2011; published 30 August 2011)

A dip-shaped anomaly appearing in the infrared spectrum of charge-transfer organic complexes has been investigated. The anomaly appears at approximately the same frequency ($\sim 2700\text{ cm}^{-1}$), irrespective of light polarization as well as a composition of the complex, when the compounds undergo charge ordering. Isotope-shift measurements for θ -(BEDT-TTF)₂RbZn(SCN)₄ [BEDT-TTF = bis(ethylenedithio)tetrathiafulvalene] indicates a relationship between the overtone of a C=C stretching mode of the BEDT-TTF molecule and this anomalous signal. Calculations of electron-molecular vibration coupling based on a diatomic molecular dimer model reveals that the overtone is activated by an anharmonicity developed in the adiabatic potential in a charge-separated system. It is presented that numerical calculation based on the simple cluster model reproduces essential features of the experimentally obtained conductivity spectrum.

DOI: [10.1103/PhysRevB.84.064306](https://doi.org/10.1103/PhysRevB.84.064306)

PACS number(s): 71.30.+h, 78.30.Jw, 63.20.kd

I. INTRODUCTION

Strongly correlated electron systems show various unusual physical properties. For these systems, electron transfer energy is competing with those of electron-electron repulsions and electron-phonon couplings, thereby the optical transitions associated with these interactions are overlaid with each other in the spectrum or coupled to give entangled structure which is difficult to interpret. For example, in the present study we focus on an apparently dip-shaped signal in the optical conductivity spectrum, which is observed for a class of organic charge-transfer complexes with highly correlated electrons.

The signal is activated when the compounds undergo charge ordering. This phenomenon is recognized as an order-disorder transition of electrons driven by repulsive interaction of electrons.^{1,2} The Wigner-crystallization-like phase transition has been found to occur in a number of mixed-valency charge-transfer complexes with the 3/4-filled electron system, and has drawn the attention of researchers because of its intriguing properties, such as various kinds of nonlinear conduction,^{3–6} light-induced phase transitions,^{7–10} unconventional ferroelectricity,^{11–13} and a possible relation with superconductivity.^{14–20}

As we will discuss in a following section, the anomaly activated along with the charge ordering is ascribed to an overtone of a molecular vibration, activated by a vibronic coupling effect. It has been widely known for organic conductors that a strong vibronic effect called electron-molecular vibration (e-mv) coupling significantly affects the spectroscopic properties. The spectroscopic impact of the vibronic effect, such as activation of totally symmetric modes in the infrared spectrum, have been explained by a linear coupling theory, in which the vibronic effect is treated as a linear perturbation to the electronic states.^{21–25} However, the theoretical treatment does not offer us any implication on the activation of the overtone.

The aim of this paper is to extend the linear coupling theory by incorporating higher-order effects of the vibronic perturbation in order to explain the activation mechanism of the overtone. By using a simple cluster model, we have demonstrated that an anharmonicity is induced in the adiabatic potential of a charge-ordered system due to the higher-order

energy correction. We then calculate the optical conductivity to examine the influence of the higher-order modulation to the electron wave functions and confirm that the experimentally observed spectrum with the overtone signal is reasonably reproduced by the simple cluster model.

The paper is organized as follows: in Sec. II, the infrared spectra of θ -(BEDT-TTF)₂RbZn(SCN)₄ [BEDT-TTF = bis(ethylenedithio)tetrathiafulvalene] and other compounds in charge-ordered phases are summarized. It is revealed by the analysis of isotope shifts in the spectra for θ -(BEDT-TTF)₂RbZn(SCN)₄ complex that there is a relationship between the dip-shaped signal and the overtone of a C=C stretching mode of the BEDT-TTF molecule. In Sec. III, we discuss the properties of a diatomic molecular dimer at equilibrium, taking account of higher-order vibronic perturbations; Sec. III A introduces the model cluster and the corresponding Hamiltonian. Section III B presents the estimation of the adiabatic potential of the dimeric system. In Sec. III C we derive the electronic wave functions, including the vibronic effect up to the second-order perturbation, and discuss the mechanism of generation of the anharmonicity. Section IV presents the optical properties of the e-mv coupled system. Section IV A is dedicated to the derivation of the optical conductivity taking account of the effect of the above-obtained perturbed wave function. In Sec. IV B we discuss features of the spectrum calculated from the optical conductivity and compare the numerical spectrum and the experimentally obtained one. Next we discuss the physical implications of the activation of the overtone in Sec. V. Finally, we summarize the present study in the last section.

II. DIP-SHAPED STRUCTURE IN INFRARED SPECTRA

Figures 1(a) and 1(b) show the polarized optical conductivity spectra of θ -(BEDT-TTF)₂RbZn(SCN)₄. This compound undergoes a metal-to-insulator transition around 190 K due to charge ordering.^{2,26–32} The two panels display the spectra measured above (300 K) and below (6 K) the phase-transition temperature. As shown by the plots, the spectra show a drastic change; the smooth profiles are transformed to the pattern

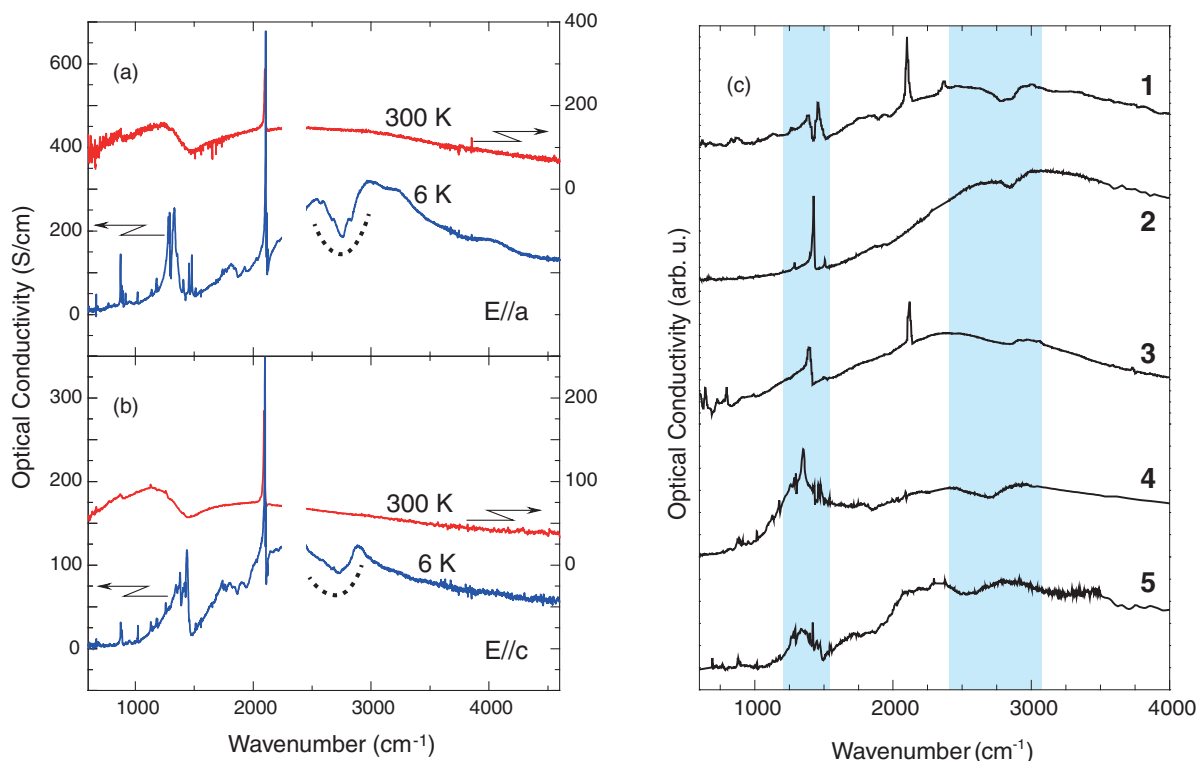


FIG. 1. (Color online) Polarized optical conductivity spectra of θ -(BEDT-TTF) $_2$ RbZn(SCN) $_4$ [(a) E//a, (b) E//c]. The two curves in each panel depict data measured at 300 and 6 K. The dotted lines indicate the dip-shaped anomaly. (c) Optical conductivity spectra of selected organic compounds in the charge-ordered state [1: θ -(BEDT-TTF) $_2$ TlZn(SCN) $_4$ (Ref. 36), 2: β' -(BEDT-TTF)(TCNQ) (Ref. 38), 3: θ -(BDA-TTP) $_2$ Cu(NCS) $_2$ (Ref. 37), 4: α -(BEDT-TTF) $_2$ I $_3$ (Ref. 12), 5: α' -(BEDT-TTF) $_2$ IBr $_2$ (this work)]. The highlighted regions of higher and lower frequency indicate the dip-shaped anomaly and the fundamental signals of C=C stretching modes, respectively.

overlaid with numerous sharp peaks as well as the apparently dip-shaped anomaly around 2700 cm^{-1} .

The sharp peaks are attributable to intramolecular vibrations because of the narrow shapes. In a previous study, we discussed the interpretation of the vibrational signals appearing in the C=C stretching region (~ 1000 – 1600 cm^{-1}) in an investigation of the inhomogeneous charge distribution associated with the transition.²⁹ While we assigned the C=C stretching signals in that study, the remaining signals were not fully investigated. Among these remaining signals, we focus on the characteristic dip-shaped anomaly here.

The anomaly could be interpreted as a valley between two or more electronic transition bands with different peak energies.^{33–35} Since large charge separation can be induced by the charge ordering, it is expected that the electronic transition band is split into several parts reflecting the multiplication of inequivalent molecules due to the charge disproportionation. Nevertheless, such an interpretation could be questioned in several ways. For example, this material is a two-dimensional complex, and thus the electron absorption energy should be dependent on the light polarization according to an anisotropy of the band dispersion; therefore, if the anomaly is associated with the electronic transitions, the signal would show significant polarization dependence. In reality, however, while the center of the spectral weight of the broad charge-transfer bands shows the noticed polarization dependence, the anomaly appears at nearly the same frequency irrespective of light polarizations, as shown in Figs. 1(a) and 1(b). Moreover, similar anomalies are

found in other organic conductors that undergo charge ordering, as shown in Fig. 1(c).^{12,36–38} Although these compounds are composed of different counterions or donor molecules, or have different chemical stoichiometry, the conductivity spectra all show a similar anomalous feature around the same frequency region. The common energy nature irrespective of the crystal structure and the composition of the compounds suggests that the signal would not be attributed to electronic transitions, but implies that the signal is related to a discrete transition having a characteristic energy such as the excitation of a molecular vibration.

Although no characteristic absorption mode exists around the frequency of the anomaly, it is noticed that the dip structure is located near the twofold frequency of the intense vibronic signal of a C=C stretching mode which appears as the positive band around ~ 1400 cm^{-1} . Comparison of the spectra shown in Fig. 1(c) allows us to recognize that there is an approximately linear relationship between the frequency of the dip-shape signal and that of the fundamental mode in each spectrum; i.e., for the spectrum in which the fundamental signal appears at a lower frequency than that of the other spectra, the dip-shape signal has a lower frequency in comparison to the other spectra. These facts suggest that the anomaly may be related to an overtone of the molecular vibration.

To examine this interpretation, we focused on the isotope shift of the dip-shape signal. Figures 2(b) and 2(c) show the conductivity spectra measured for a normal crystal of θ -(BEDT-TTF) $_2$ RbZn(SCN) $_4$ and an isotope-labeled sample

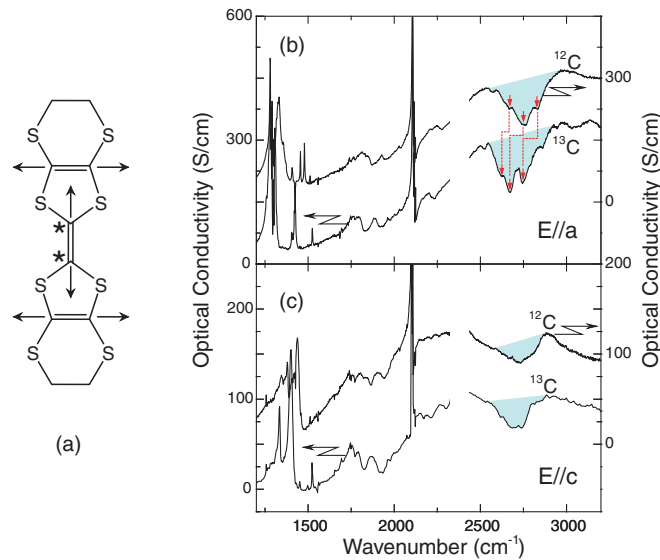


FIG. 2. (Color online) (a) Molecular structure of the BEDT-TTF molecule. The asterisks denote the carbon atoms replaced by ^{13}C for the isotope-shift measurement. The arrows denote the C=C stretchings in the $\nu_3(a_g)$ mode. (b) and (c) Polarized optical conductivity spectra measured from the normal (^{12}C) and the isotope labeled (^{13}C) θ -(BEDT-TTF) $_2\text{RbZn}(\text{SCN})_4$ [(b) E//a, (c) E//c]. The highlighted regions indicate the dip-shaped anomaly. The vertical arrows in (b) denote the isotope shift of several vibrational structures in the dip structure.

composed of BEDT-TTF molecules in which two central carbon atoms were replaced with ^{13}C [Fig. 2(a)], respectively. It was found that there were appreciable differences between these two profiles. For example, several small structures in the dip structure were displaced, as marked by arrows. Moreover, the dip structure itself showed a sizable isotope shift. By assuming that the average frequency of the dip region is given by $\langle\omega_{\text{dip}}\rangle = \int \omega\sigma(\omega)d\omega / \int \sigma(\omega)d\omega$ [as marked by the highlighted area in Figs. 2(b) and 2(c)], it was estimated that the dip signal was displaced from $\sim 2757\text{ cm}^{-1}$ to $\sim 2731\text{ cm}^{-1}$ in the spectrum for E//a, and from 2729 cm^{-1} to 2709 cm^{-1} for E//c. These isotope shifts are a clear indication that the dip signal is related to the C=C stretching mode. From the twofold frequency of the fundamental signal, we proposed that the dip is attributable to the overtone of the stretching mode.

Generally, overtones are activated by some anharmonicity in the vibrational potential. In the present case, however, most organic conductors, except for the compounds such as those included in Fig. 1(c), do not show an anomalous signal. Thus, it is suggested that individual BEDT-TTF molecules should not have significant anharmonicity in the potential for the C=C stretching mode. On the other hand, it is known that the C=C stretching mode is strongly coupled with conduction electrons by the e-mv coupling effect. This fact suggests that the anharmonicity may arise from the vibronic effect in a limited condition that is probably connected with the charge ordering.

To evaluate such a proposition, we investigate the adiabatic potential and the optical conductivity of a charge-ordered system using a simple cluster model. In the following section, we describe the theoretical treatments of the model calculation; afterward we present the results of a numerical simulation of the experimentally obtained conductivity spectrum based on the simple model.

III. DIATOMIC MOLECULAR DIMER MODEL AND ADIABATIC PROPERTIES

The e-mv coupling effect can be regarded as an energy shift of the valence level associated with totally symmetric molecular vibrations. When two molecules oscillate in the out-of-phase manner, a conduction electron will hop between the molecules in accordance with dynamical oscillation of the valence levels caused by the e-mv coupling. As the result of such electron hopping, the originally infrared-forbidden mode is activated in the optical conductivity spectrum. To describe the spectroscopic properties associated with the vibronic effect, therefore, a model system requires at least two molecules, each of which should have at least one molecular normal coordinate like a diatomic molecule, and should have one radical electron in the dimeric unit.

We investigate the e-mv coupling phenomena for a system in a charge-ordered state using such a diatomic molecular cluster model. Since our focus is mainly on 3/4-filled cationic complexes (having a hole per two molecules), we place a hole in the cluster instead of an electron. We will see that this simple model is instructive for a qualitative understanding of the vibronic activation of the overtone. Moreover, the model is effective for a numerical analysis of the experimentally observed optical conductivity spectrum.

A. Hamiltonian and eigenstates of an unperturbed system

The total Hamiltonian of an electron-phonon coupled system under an external electric field is expressed by $H = H_e + H_v + H_{\text{emv}} + H_F(t)$, where H_e and H_v denote the Hamiltonian for the pure-electron and vibrational states, and H_{emv} and $H_F(t)$ represent the e-mv coupling and the external-field effect, respectively. The electronic Hamiltonian for the dimeric cluster is written as $H_e = \Delta\epsilon n_1 - \Delta\epsilon n_2 -$

$t(|1\rangle\langle 2| + |2\rangle\langle 1|)$, where n_1 and n_2 denote the charge density (hole density in the present discussion) operators for molecules 1 and 2, respectively. $|1\rangle$ and $|2\rangle$ are the respective electron wave functions in the bra-ket notation, and t is the transfer energy between the two molecules. As mentioned earlier, we are interested in the charge ordering driven by intersite electron-electron repulsions. In the present cluster model, we introduce the electron correlations effect via the difference in the site energy ($\pm\Delta\varepsilon$).

The ground and excited states of the two-level dimer system can be formally written as

$$\begin{aligned} |g\rangle &= c_1|1\rangle + c_2|2\rangle, \\ |e\rangle &= c_2|1\rangle - c_1|2\rangle, \end{aligned} \quad (3.1)$$

where $c_1^2 + c_2^2 = 1$. If we denote the charge separation of the pure-electronic ground state as $\delta\rho$ ($= \langle g|n_1 - n_2|g\rangle = \langle g|\delta n|g\rangle = c_1^2 - c_2^2$), the transition matrix element δn_{eg} ($= \langle e|\delta n|g\rangle$) and the ratio between the energy gap E_{eg} ($= E_e - E_g = \langle e|H_e|e\rangle - \langle g|H_e|g\rangle$) and t are written as

$$\delta n_{eg} = \sqrt{1 - \delta\rho^2}, \quad (3.2)$$

$$\frac{E_{eg}}{t} = \frac{2}{\sqrt{1 - \delta\rho^2}}, \quad (3.3)$$

where $t > 0$. Note that in this expression, the effect of $\Delta\varepsilon$, i.e., the electron correlation, has been imposed on $\delta\rho$.

The pure vibrational Hamiltonian of the two molecules can be written

$$H_v = \sum_{i=1,2} \frac{\omega_i}{4} (\dot{Q}_i^2 + Q_i^2), \quad (3.4)$$

where Q_i denotes the dimensionless normal coordinate of the i th molecule [which is related to the usual mass-weighted coordinate (q_i) via the relationship $Q_i = \sqrt{2\omega_i}q_i$], \dot{Q}_i is the conjugated momentum of Q_i , and ω_i is the eigenfrequency of the vibration for the neutral state ($\hbar = 1$).

The e-mv coupling effect can be expressed as a dependence of the valence electron level on the molecular deformation denoted by the normal coordinate. The Hamiltonian is thus written by a power series of the electronic energy in terms of the normal coordinate of the molecular vibration, i.e.,

$$H_{emv} = \sum_{i=1,2} \left[gn_i Q_i + \frac{1}{2} g^{(2)} n_i Q_i^2 + O(Q_i^3) \right], \quad (3.5)$$

where g ($= \partial E_g / \partial Q$) and $g^{(2)}$ ($= \partial^2 E_g / \partial Q^2$) refer to the linear and quadratic coupling constants, respectively. The first term indicates the linear dependence of the valence level on Q , whereas the second term denotes the quadratic dependence. As is seen from the quadratic form, this term adds such an additional fraction to the original harmonic potential of the Q mode as the function of the molecular charge n . Hence, this effect represents the molecular ionicity dependence of the eigenfrequency of the vibrational mode.

It may be possible to repeat the power series expansion until we obtain anharmonic terms. However, one should note as mentioned earlier that individual BEDT-TTF molecules appear not to have significant anharmonicity. Therefore, it would be reasonable to exclude the effect of such higher-order terms from the discussion.

For TTF-derived molecules including BEDT-TTF, it is known that one of the C=C stretching modes called $\nu_3(a_g)$ has an exceedingly large g constant compared with the other ones.^{39–42} As we will see later, the anharmonicity generated by the vibronic coupling effect has a cubic dependence on the coupling constant. Thus, it is expected that this mode with the large g constant should play a dominant role in the vibronic coupling phenomenon. As schematically shown in Fig. 2(a), this mode includes the stretching motion of the central C=C bond. Therefore, it is expected that the eigenfrequency should be decreased by the ¹³C replacements. The low-frequency isotope shift is consistent with the experimental results discussed in Sec. II. These considerations rationalize that we have focused on only one vibrational mode in the cluster model.

For the convenience of understanding, we introduce the symmetry-adapted coordinates $Q_+ = (1/\sqrt{2})(Q_1 + Q_2)$ and $Q_- = (1/\sqrt{2})(Q_1 - Q_2)$. With the use of these coordinates, the vibronic Hamiltonian H_{emv} are rewritten as

$$\begin{aligned} H_{emv} &= \frac{Ng}{\sqrt{2}} Q_+ + \frac{g\delta n}{\sqrt{2}} Q_- + \frac{N}{4} g^{(2)} (Q_+^2 + Q_-^2) \\ &\quad + \frac{g^{(2)}}{2} \delta n Q_+ Q_-, \end{aligned} \quad (3.6)$$

in which N denotes the total charge density (i.e., $N = 1$). We will evaluate the influence of the vibronic coupling for the adiabatic potential in the next section, and then calculate the optical conductivity in the successive sections.

B. Adiabatic potential

As demonstrated by the isotope-shift measurements, the dip-shaped anomaly appears to have some connection to an overtone of the C=C stretching mode. To understand the activation mechanism of the overtone, we focus on the adiabatic potential of the dimeric system.

The vibronic modulation of the adiabatic potential is given by the series of the perturbation energies due to H_{emv} to the electronic ground state, which can be classified in terms of the order of the perturbations:

$$\begin{aligned} E^{(1)} &= \frac{gN}{\sqrt{2}} Q_+ + \frac{g\delta\rho}{\sqrt{2}} Q_- + \frac{g^{(2)}N}{4} (Q_+^2 + Q_-^2) \\ &\quad + \frac{g^{(2)}}{2} \delta\rho Q_+ Q_-, \end{aligned} \quad (3.7)$$

$$E^{(2)} = -\frac{g^2 \delta n_{ge}^2}{2E_{eg}} Q_-^2 - \frac{gg^{(2)} \delta n_{ge}^2}{\sqrt{2}E_{eg}} Q_+ Q_-^2 + O(Q^4), \quad (3.8)$$

$$E^{(3)} = -\frac{g^3 \delta n_{ge}^2 \delta\rho}{\sqrt{2}E_{eg}^2} Q_-^3 + O(Q^4), \quad (3.9)$$

where the superscripts of E denote the order of the perturbation. The first and second terms in Eq. (3.7) indicate linear energy shifts depending on Q_+ and Q_- , which give rise to displacements of the equilibrium positions of the respective coordinates. The third term in Eq. (3.7) represents the renormalization of the eigenfrequency from the values for the neutral molecule to that for the average charge density ($+e/2$).

For a system with nonzero charge separation ($\delta\rho \neq 0$), the Q_+ and Q_- modes are no longer the eigenmodes of the system. The fourth term in Eq. (3.7) denotes the mixing of the two modes due to the charge separation that breaks the symmetry of the dimer. The square term of Q_- in the second-order perturbation [Eq. (3.8)] represents a low-frequency shift of the out-of-phase mode.

While most studies on the e-mv coupling effects have neglected the remaining higher-order terms, we have examined the spectroscopic influence of these higher-order terms. One can see that there are two cubic (the lowest-order anharmonicity) terms in the perturbation energy, i.e., the second term in Eq. (3.8) and the first term in Eq. (3.9). The former term denotes an anharmonic interaction between Q_+ and Q_- . As can be seen from the numerator of Eq. (3.8), this term essentially consists of the transition matrix elements δn_{ge} , thus there should be a finite contribution of this term for any systems having nonzero charge-transfer matrix elements. On the other hand, the latter term includes the charge separation $\delta\rho$, indicating that this term represents the anharmonicity characteristic for the system with charge separation.

To compare the magnitude of the two anharmonicities, we evaluated the coefficients of the two terms

$$A_{CT} = \left| \frac{gg^{(2)}\delta n_{ge}^2}{\sqrt{2}E_{eg}} \right|, \quad (3.10)$$

$$A_{CD} = \left| \frac{g^3\delta n_{ge}^2\delta\rho}{\sqrt{2}E_{eg}^2} \right|. \quad (3.11)$$

The coefficient A_{CT} is the factor for the second term in Eq. (3.8), which is associated with charge-transfer interaction and A_{CD} refers to the coefficient for the first term in Eq. (3.9), which is thus related to charge disproportionation.

To evaluate the two anharmonic terms, one must know the e-mv coupling constants g and $g^{(2)}$ in advance. The linear coupling constant g of the BEDT-TTF molecule has been calculated by various studies.^{39–42} For example, according to the latest study (Ref. 42), the g constant for the ν_3 mode is estimated as 132 meV. On the other hand, as mentioned in Sec. III A, the quadratic coupling constant $g^{(2)}$ can be determined from the frequency difference between the neutral and ionic states. For a donor molecule, for instance, the coefficient is given by using the vibrational frequencies of the neutral (ω_{neutral}) and cationic (ω_{cation}) states, as

$$g^{(2)} = \frac{1}{2}(\omega_{\text{cation}} - \omega_{\text{neutral}}). \quad (3.12)$$

For the $\nu_3(a_g)$ mode, ω_{neutral} and ω_{cation} have been reported to be 1494 and 1415 cm^{-1} , respectively.^{41,43–45} From these values, $g^{(2)}$ was determined to be 5.6 meV (45 cm^{-1}).

The remaining parameters to be specified are $\delta\rho$, δn_{ge} , E_{eg} , and t . For a given $\delta\rho$, δn_{ge} is explicitly determined via Eq. (3.2), whereas E_{eg} and t are given by a relative value as the function of $\delta\rho$ by Eq. (3.3). We thus have calculated these coefficients in two different ways: by fixing E_{eg} and by fixing t . Figure 3 shows the results of the two calculations. Panel (a) depicts the coefficients calculated as the function of $\delta\rho$ for a fixed t , whereas panel (c) shows the result for a fixed E_{eg} . In both plots, the A_{CD} term (the anharmonicity related

to charge disproportionation) grows from zero with increasing $|\delta\rho|$, forming broad peaks for $|\delta\rho| = 0.3\text{--}0.7$, then decreases for $|\delta\rho| \rightarrow 1$. Meanwhile, the A_{CT} term, which is related to charge transfer, has the maximum at $\delta\rho = 0$ and monotonically decreases its intensity down to zero with increasing $|\delta\rho|$.

As demonstrated by the ratio plots in Figs. 3(b) and 3(d), the magnitude of A_{CD} is much larger than that of A_{CT} for most values of $\delta\rho$. In the region where A_{CD} forms a broad peak ($|\delta\rho| = 0.3\text{--}0.7$), this coefficient dominates A_{CT} . This strongly suggests that the anharmonicity associated with the A_{CD} term, i.e., the third-order perturbation energy, played an essential role in the activation of the overtone in charge-ordered systems.

C. Vibronic perturbation of electron wave functions

To understand the generation mechanism of the anharmonicity associated with A_{CD} , we focus on the vibronic modulation of the electronic wave functions. Generally, the third-order energy perturbation is related to the second-order perturbation of the wave functions, thus we deal with the vibronic perturbations up to the second-order corrections.

Within the adiabatic approximation, the perturbation expansions of the electronic wave functions are written as

$$|\Psi_g\rangle = |g\rangle - \frac{g\delta n_{eg}Q_-}{\sqrt{2}E_{eg}}|e\rangle - \frac{g^2\delta\rho\delta n_{eg}Q_-^2}{E_{eg}^2}|e\rangle - \frac{g^2\delta n_{eg}^2Q_-^2}{4E_{eg}^2}|g\rangle, \quad (3.13)$$

$$|\Psi_e\rangle = |e\rangle - \frac{g\delta n_{eg}Q_-}{\sqrt{2}E_{eg}}|g\rangle - \frac{g^2\delta\rho\delta n_{eg}Q_-^2}{E_{eg}^2}|g\rangle - \frac{g^2\delta n_{eg}^2Q_-^2}{4E_{eg}^2}|e\rangle. \quad (3.14)$$

For the derivation, we have simplified the perturbation Hamiltonian H_{emv} [Eq. (3.6)] to

$$H_{\text{emv}} = \frac{g\delta n}{\sqrt{2}}Q_-, \quad (3.15)$$

because the omitted terms do not include the charge-transfer operator δn , which is involved in the anharmonic coefficient A_{CD} as the form of the charge separation $\delta\rho$ or the transition matrix element δn_{eg} , or have the coefficient $g^{(2)}$, which is much smaller than g .

The obtained wave functions [Eqs. (3.13) and (3.14)] are composed of the original wave functions and the modulation terms. The second terms in the wave functions arise from the first-order correction to the wave function. Its spectroscopic effect would be transparent; in the case for the ground-state wave function, for example, the correction gives rise of the mixing of the excited level to the ground state depending on Q_- . On the other hand, the influence of the third and fourth terms in Eq. (3.13), which are attributed to the second-order correction of the wave function, may not be clear because of the complexities of the form, i.e., they are quadratically proportional to Q_- and related to both the ground and excited states.

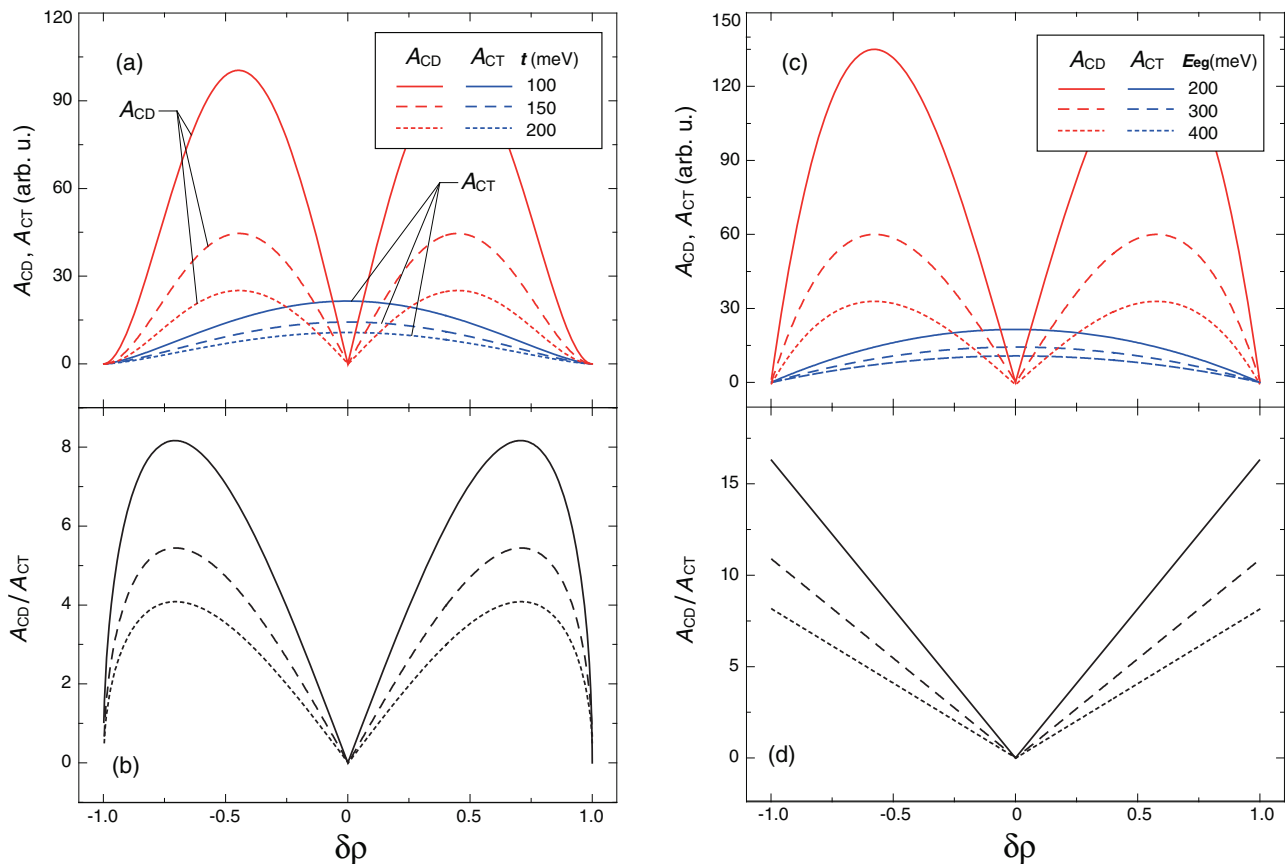


FIG. 3. (Color online) Two types of vibronically induced anharmonicity [A_{CD}, A_{CT} (see text)] calculated as a function of charge separation $\delta\rho$ ($g = 132$ meV, $g^{(2)} = 0.56$ meV). (a) and (c) show the results calculated for constant t and constant E_{eg} , respectively. (b) and (d) show the ratio between the two anharmonicities of the respective calculations.

To aid in understanding, we calculate the expectation value of charge separation using the modified wave function. The value is given by

$$\langle \Psi_g | \delta n | \Psi_g \rangle = \delta\rho - \frac{\sqrt{2}g\delta n_{eg}^2}{E_{eg}} Q_- - \frac{3g^2\delta n_{eg}^2\delta\rho}{E_{eg}^2} Q_-^2. \quad (3.16)$$

In this expression, the second term in the right-hand side arises from the first-order correction to the wave function, whereas the third term, which has the quadratic dependence on Q_- , stems from the second-order corrections. At equilibrium, the stationary value of Q_- can be determined from the condition of $\partial E / \partial Q_- = 0$, where E denotes the adiabatic potential of the ground state. From the energy correction given by Eq. (3.7) and the vibrational Hamiltonian of Eq. (3.4), we find $Q_- = -\sqrt{2}g\delta\rho/\omega_{avg}$ [where $\omega_{avg} = (1/2)(\omega_{cation} + \omega_{neutral})$]. With the replacement of Q_- with this equilibrium value, Eq. (3.16) is rewritten for a given $\delta\rho$ as

$$\begin{aligned} \langle \Psi_g | \delta n | \Psi_g \rangle &= \delta\rho + \left(\frac{2g^2\delta n_{eg}^2}{\omega_{avg}E_{eg}} \right) \delta\rho - \left(\frac{2g^2\delta n_{eg}^2}{\omega_{avg}E_{eg}} \right) \\ &\times \left(\frac{3g^2}{\omega_{avg}E_{eg}} \right) \delta\rho^3. \end{aligned} \quad (3.17)$$

The second and third terms in the expression are attributed to the effect of the first-order and second-order corrections of the wave function, respectively.

Using Eq. (3.17), we have evaluated the expectation value of charge separation at equilibrium state as the function of the original charge separation. As performed in the calculations of the anharmonic coefficients (Fig. 3), this calculation has been carried out in two ways: for a fixed t and for a fixed E_{eg} . Figures 4(a) and 4(c) show the respective results, and the accompanying Figs. 4(b) and 4(d) display the modulated part of the charge separation extracted from the expectation value ($\langle \Psi_g | \delta n | \Psi_g \rangle - \delta\rho$).

It would be evident from the form of Eq. (3.17) that the coefficient of the second term is always positive, thus it should enhance the charge separation in proportion to the original (pure-electronic) value $\delta\rho$. It is illustrated that the first-order correction [the second term in Eq. (3.17)] enhances the charge separation as shown by the solid lines in Fig. 4. As shown by Figs. 4(b) and 4(d), the enhancement develops with increasing $|\delta\rho|$, forming the broad maximum around the middle point of $|\delta\rho|$ (~ 0.5), and then approaches zero for $|\delta\rho| \rightarrow 1$.

It is noted that the charge separation modulated by this term exceeds unity for $|\delta\rho| \sim 0.8$, as shown in Fig. 4(c). Such excessive modulation of charge separation is corrected by the effect of the second-order perturbation to the wave function;

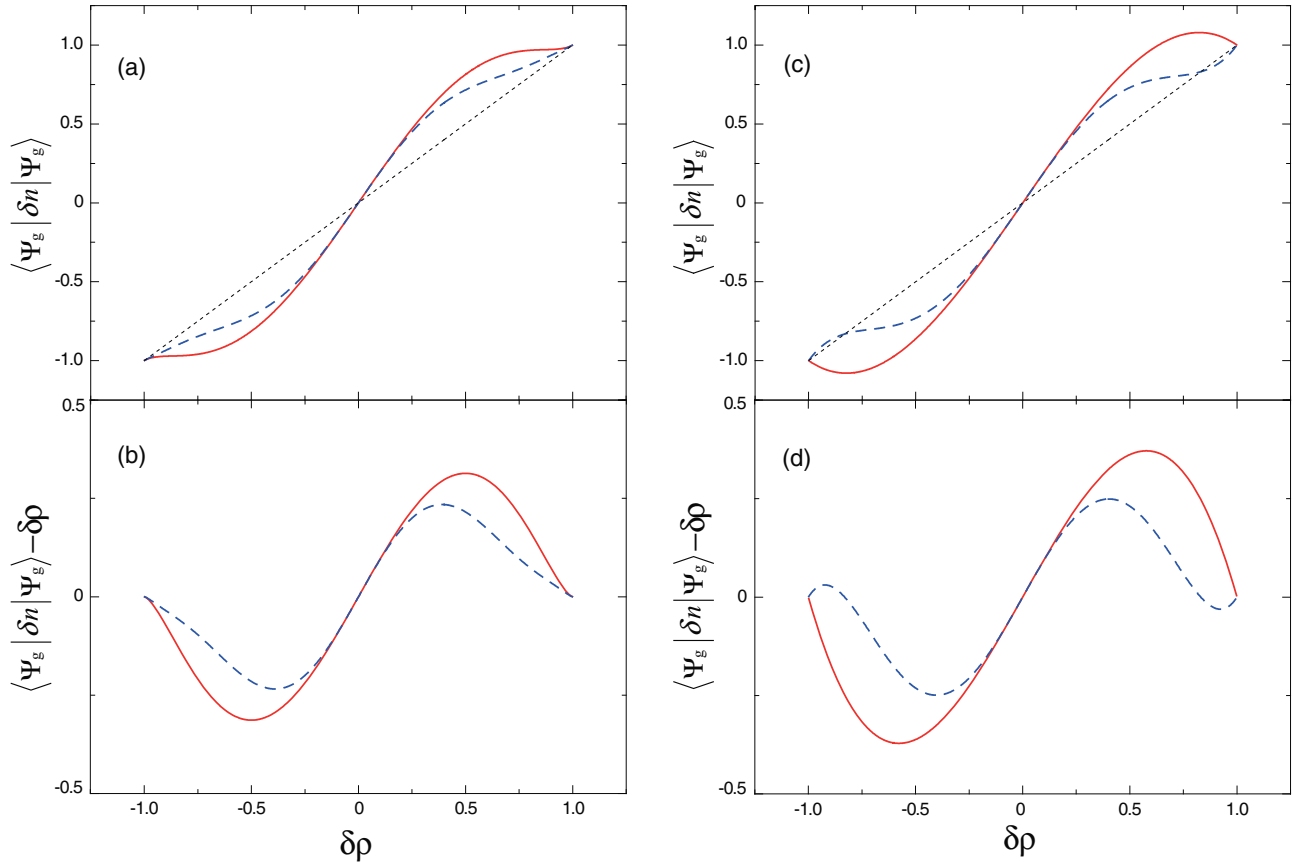


FIG. 4. (Color online) The charge separation modulated by the e-mv coupling, plotted as a function of the original (pure-electronic) charge separation $\delta\rho$ ($g = 132$ meV). (a) and (c) show the results calculated for constant t ($= 100$ meV) and for constant E_{eg} ($= 200$ meV), respectively. (b) and (d) display the difference between the modulated charge separation and the original one for the results shown in (a) and (c), respectively. The solid curves denote the charge separation modulated by the first term in Eq. (3.17), whereas the dashed curves include the modulation due to the second term in the equation (see text).

as shown by the dashed lines, the charge separation including the second-order correction effect is adjusted to a reasonable range. As is suggested from such a function, the influence of the second-order corrections is intensified for a middle region of $|\delta\rho|$ where the vibronic enhancement of charge separation is strengthened. It should be noted that such $\delta\rho$ dependence agrees well with that of the anharmonicity characterized by A_{CD} .

The enhanced modulation of charge separation indicates strong coupling between the electronic states and the molecular vibration at equilibrium, which in turn means that the potential of the molecular vibration, which behaves otherwise as a harmonic oscillator, should be largely distorted by the broken symmetry of the charge-separated system. Therefore, it would be a natural consequence that an anharmonicity is induced in the system having large charge separation.

IV. OPTICAL PROPERTIES

A. Expression of optical conductivity

To examine the influence of the anharmonicity to spectroscopic properties, we investigate the optical conductivity spectrum using the dimeric model. For a pure electronic dimeric

system, in which the charge-transfer operator is coupled with an external field via the time-dependent Hamiltonian,

$$H_F(t) = -\frac{ea}{2}\delta n F(t), \quad (4.1)$$

where a , e , and $F(t)$, respectively denote the intermolecular distance, electron charge, and electric field, the electric susceptibility $\chi_{elec}(\omega)$ [in the present discussion, we defined it as $\chi_{elec}(\omega) = \delta n(\omega)/F(\omega)$] is given by

$$\chi_{elec}(\omega) = \sum_n \frac{2\omega_{ng} \langle n | \delta n | g \rangle^2}{\omega_{ng}^2 - \omega^2 - 2i\omega\gamma}, \quad (4.2)$$

where n , γ , and ω represent the quantum number of the excited state, the phenomenological damping factor of the electronic states, and the frequency of the electric field, respectively.

In the present vibronic system, on the other hand, δn is also coupled with the vibrational coordinate Q_- . So far, we have supposed the coordinate to be a static parameter in terms of the adiabatic approximation. In fact, however, the coordinates should vary with time. Thus, we have to treat it as a time-dependent parameter, and then solve the problem of simultaneous differential equations.

In Ref. 22, this problem has been addressed by considering the vibronic contribution as an effective time-dependent field

to the electronic system with the following steps: first, the coordinate Q_- has been supposed to be driven by the time dependence of the charge density δn via the vibronic Hamiltonian [Eq. (4.1)]. The susceptibility of the mode $[\chi_{Q_-}(\omega)]$, which is defined as

$$Q_-(\omega) = \chi_{Q_-}(\omega)\delta n(\omega), \quad (4.3)$$

has been obtained from the equation motion of the harmonic oscillator in classical mechanics. Within the first-order time-dependent perturbation theory, there should be an electric susceptibility $\chi_{\text{total}}(\omega)$ (i.e., the solution of the present problem) that allows us to express the charge density of the total system as a linear function of the external field $F(\omega)$, i.e.,

$$\delta n(\omega) = \chi_{\text{total}}(\omega)F(\omega). \quad (4.4)$$

By the replacement of $\delta n(\omega) \rightarrow \chi_{\text{total}}(\omega)F(\omega)$, Eq. (4.3) is rewritten as $Q_-(\omega) = \chi_{Q_-}(\omega)\chi_{\text{total}}(\omega)F(\omega)$. With the help of the transformation, the vibronic Hamiltonian can be unified with the external field effect [Eq. (3.15)] to give

$$\begin{aligned} H'(\omega) &= H_{\text{emv}}(\omega) + H_F(\omega) \\ &= \delta n \left[\left(\frac{g}{\sqrt{2}} \chi_{Q_-}(\omega)\chi_{\text{total}}(\omega) - \frac{ea}{2} \right) F(\omega) \right]. \end{aligned} \quad (4.5)$$

This formula states that the square bracketed part, composed of the external field and the molecular vibration excited by the vibronic coupling, may work as an effective field to the pure electronic system. Using the replacement of $F(\omega) \rightarrow [(g/\sqrt{2})\chi_{Q_-}(\omega)\chi_{\text{total}}(\omega) - (ea/2)]F(\omega)$ in the derivation of Eq. (4.4), we obtain

$$\delta n(\omega) = \chi_{\text{elec}}(\omega)[(g/\sqrt{2})\chi_{Q_-}(\omega)\chi_{\text{total}}(\omega) - (ea/2)]F(\omega) \quad (4.6)$$

by first-order time-dependent perturbation theory. A comparison of this result with Eq. (4.4) leads to the following:

$$\chi_{\text{total}}(\omega) = \frac{(-ea/2)\chi_{\text{elec}}(\omega)}{1 - (g/\sqrt{2})\chi_{Q_-}(\omega)\chi_{\text{elec}}(\omega)}. \quad (4.7)$$

Note that within the above treatment, the vibronic effect, which is included in Eq. (4.5) as the effective field to the electronic system, is involved in only one perturbation procedure, i.e., when Eq. (4.6) is derived. Thus, the resultant electric susceptibility does not include the second-order perturbation effect that we discussed in Sec. III. In order to investigate the optical response associated with the overtone within the framework in Ref. 22, one has to somehow perform an additional perturbation procedure to incorporate the second-order contribution.

There would be several ways to carry out the perturbation procedure. A direct way, for example, would be to apply the vibronic perturbation to the electronic wave functions. However, the physical meaning of wave function, and thus the effect of its modulation, may be uneasy to understand (therefore, we calculated the expectation value of charge separation in Sec. III C). For convenience in understanding, we have tried to impose the perturbation effect to the Hamiltonian by the following procedure.

To this end, we focus on the modification of the transition matrix element that defines the electric susceptibility

[Eq. (4.2)]. If we replace the pure electronic wave functions $|g\rangle$ and $|e\rangle$ to the vibronically perturbed ones $|\Psi_g\rangle$ and $|\Psi_e\rangle$ the transition moment is modified to

$$\langle \Psi_e | \delta n | \Psi_g \rangle = \langle e | \left(1 - \frac{\sqrt{2}g\delta\rho}{E_{\text{eg}}} Q_- \right) \delta n | g \rangle, \quad (4.8)$$

where we have excluded the modulation terms except for the linear one. By neglecting the modulations of the denominator in Eq. (4.2) due to the e-mv coupling, we find that the adiabatic perturbation to the wave function can approximately be regarded as the replacement of the charge-transfer operator δn to $[1 - (\sqrt{2}g\delta\rho/E_{\text{eg}})Q_-]\delta n$.

By the replacement of the charge-transfer operator, the vibronic Hamiltonian of Eq. (3.15) is modified to

$$H_{\text{emv}} = \frac{g}{\sqrt{2}}\delta n Q_- - \frac{g^2\delta\rho}{E_{\text{eg}}}\delta n Q_-^2. \quad (4.9)$$

Note that the second term in the Hamiltonian represents the linear coupling term between the charge transfer δn and the overtone of the Q_- mode in Eq. (4.2), suggesting the appearance of influence of the overtone in the electric susceptibility derived by the above-mentioned time-dependent perturbation treatment.

While in Ref. 22 the susceptibility $\chi_{Q_-}(\omega)$ has been given from the equation of motion of the harmonic oscillator in classical mechanics, here we employ the quantum mechanics for the simple description of the overtone. If we assume that the fundamental Q_- and its harmonic modes Q_-^2 are driven by the time-dependent modulation of δn , the susceptibilities of the respective modes, i.e., $\chi_{Q_-}(\omega)$ and $\chi_{Q_-^2}(\omega)$ [defined as $Q_-^2(\omega) = \chi_{Q_-^2}(\omega)F(\omega)$], can be obtained in a similar process to that performed in the derivation of Eq. (4.2) from Eq. (4.1). In this procedure, one must note that the symmetry-adapted modes Q_+ and Q_- are mixed to form new eigenstates in the system with charge separation. Using the new eigenstates as the basis of the matrix elements, $\chi_{Q_-}(\omega)$ and $\chi_{Q_-^2}(\omega)$ may be written as

$$\chi_{Q_-}(\omega) = \sum_n \left(\frac{g}{\sqrt{2}} \right) \frac{2\Omega_{ng} |\langle \Phi_n | Q_- | \Phi_g \rangle|^2}{\Omega_{ng}^2 - \omega^2 + 2i\omega\Gamma}, \quad (4.10)$$

$$\chi_{Q_-^2}(\omega) = \sum_n \left(-\frac{g^2\delta\rho}{E_{\text{eg}}} \right) \frac{2\Omega_{ng} |\langle \Phi_n | Q_-^2 | \Phi_g \rangle|^2}{\Omega_{ng}^2 - \omega^2 + 2i\omega\Gamma}, \quad (4.11)$$

where Φ denotes the vibrational eigenstates for the state with $\delta\rho$, Γ represents the damping factor of the vibrational states, and Ω_{ng} stands for the frequency difference between the n th excited and the ground level of the vibrational state. In fact, the index n should be composed of two parameters to specify the two orthogonal vibrational modes. If we denote the eigenmodes as R and S , and the respective indices as n_R and n_S , then the vibrational wave functions are expressed as $|\Phi_n\rangle = |n_R\rangle|n_S\rangle$ (i.e., the ground state $|\Phi_g\rangle$ is $|n_R = 0\rangle|n_S = 0\rangle$).

On the other hand, the operator of Q_- is transferred to a linear combination of the R and S modes as

$$Q_- = \zeta R + \xi S \quad (4.12)$$

[the coefficients ζ and ξ are determined in the Appendix]. Substituting the operators R and S by the annihilation and creation operators, i.e., $R \rightarrow b_R - b_R^\dagger$ and $S \rightarrow b_S - b_S^\dagger$, we can evaluate the matrix elements in the summation of Eqs. (4.10) and (4.11). Since the elements from the vibrational ground state are given from the selection rules for the quantum harmonic oscillator ($n > 0$),

$$\langle n | X | 0 \rangle = \langle n | b_X - b_X^\dagger | 0 \rangle = \begin{cases} 0 & (n \neq 1) \\ -1 & (n = 1) \end{cases}, \quad (4.13)$$

$$\begin{aligned} \langle n | X^2 | 0 \rangle &= \langle n | b_X^2 - b_X b_X^\dagger - b_X^\dagger b_X + b_X^{\dagger 2} | 0 \rangle \\ &= \begin{cases} 0 & (n \neq 2) \\ \sqrt{2} & (n = 2) \end{cases}, \end{aligned} \quad (4.14)$$

where $X = R$ or S , we find the descriptions of the susceptibilities of the Q_- and Q_-^2 modes,

$$\chi_Q(\omega) = \frac{2\Omega_R \zeta^2}{\Omega_R^2 - \omega^2 + 2i\omega\Gamma} + \frac{2\Omega_S \xi^2}{\Omega_S^2 - \omega^2 + 2i\omega\Gamma}, \quad (4.15)$$

$$\begin{aligned} \chi_{QQ}(\omega) &= \frac{4\Omega_R \zeta^4}{(2\Omega_R)^2 - \omega^2 + 2i\omega\Gamma} + \frac{4(\Omega_R + \Omega_S) \zeta^2 \xi^2}{(\Omega_R + \Omega_S)^2 - \omega^2 + 2i\omega\Gamma} \\ &+ \frac{4\Omega_S \xi^4}{(2\Omega_S)^2 - \omega^2 + 2i\omega\Gamma}, \end{aligned} \quad (4.16)$$

where Ω_X stands for the eigenfrequency of the X mode ($X = R$ or S). For simplicity, we have supposed that each mode has a common damping factor Γ .

As the result of the variation of the vibronic Hamiltonian, the time-dependent Hamiltonian Eq. (4.5) is rewritten lead

$$\begin{aligned} H'(\omega) &= H_{\text{env}}(\omega) + H_F(\omega) \\ &= \delta n \left[\frac{g}{\sqrt{2}} Q_-(\omega) - \frac{g^2 \delta \rho}{E_{\text{eg}}} Q_-^2(\omega) - \frac{ea}{2} F(\omega) \right]. \end{aligned} \quad (4.17)$$

As argued above, by assuming the square brackets in the equation to be a time-dependent perturbation to the pure electronic system, one finds that the total electron susceptibility in Eq (4.7) is modified to

$$\chi_{\text{total}}(\omega) = \frac{(-ea/2)\chi_{\text{elec}}(\omega)}{1 - (g/\sqrt{2})\chi_Q(\omega)\chi_{\text{elec}}(\omega) - (g^2\delta\rho/E_{\text{eg}})\chi_{QQ}(\omega)\chi_{\text{elec}}(\omega)}. \quad (4.18)$$

Note that the vibronic effects associated with the overtones are involved together with that of the fundamental mode in the denominator. It should be noted that the two contributions are expressed in the equivalent form, i.e., the product between the vibrational (χ_Q or χ_{QQ}) and the pure-electronic susceptibilities (χ_{elec}), aside from the difference in the coefficients. This equivalence implies that the overtone should show spectroscopic features similar to those of the fundamental signals.

According to the present definition of the complex electric susceptibility, the imaginary part of the dielectric constant is expressed as $\varepsilon'' = N_{\text{dimer}}(-ea/2)\text{Im} \chi_{\text{total}}$, where N_{dimer} is the density of the dimeric units in the unit volume. Thereby, the optical conductivity (defined as $\sigma = -\omega\varepsilon''$) is given by²²

$$\sigma(\omega) = -\omega N_{\text{dimer}} \left(-\frac{ea}{2} \right) \text{Im} \chi_{\text{total}}(\omega). \quad (4.19)$$

B. Numerical spectra and simulation

Figures 5(a)–5(c) show the optical conductivity spectra of the dimeric model calculated by Eq. (4.19). Figure 5(a) depicts the conductivity spectra calculated for various $\delta\rho$ with a fixed E_{eg} , as in the case for Fig. 3(c), whereas Fig. 5(b) shows the t dependence of the spectra calculated in a similar way in Fig. 3(c), respectively. The spectra in Fig. 5(c) have been calculated for various g constants. Parameters used in each calculation are displayed in the panels (common parameters: $\omega_{\text{neutral}} = 1494 \text{ cm}^{-1}$,⁴³ $\omega_{\text{cation}} = 1407 \text{ cm}^{-1}$,⁴⁴ $\Gamma = 100 \text{ cm}^{-1}$, and $\gamma = 1000 \text{ cm}^{-1}$).

The calculated spectra commonly displayed a very broad band due to the charge transfer between the molecules. In

Fig. 5(a), we have shown the spectrum calculated without vibronic coupling (dashed line: $g = 0, \delta\rho = 0$). The comparison between the pure-electronic spectrum and the curve calculated with the coupling effect (black solid line: $g = 120 \text{ cm}^{-1}$, $\delta\rho = 0$) illustrates that the spectral weight for the spectral region above the fundamental frequency [$1450.5 \text{ cm}^{-1} = (\omega_{\text{neutral}} + \omega_{\text{cation}})/2$] is flown to the lower-frequency region in accordance with the low-frequency shift of the Q_- mode as mentioned in Sec. III B, resulting in the formation of such antiresonance structures²³ (spreading from ~ 1000 to $\sim 3000 \text{ cm}^{-1}$) as those observed for the system in which a discrete level is coupled with continuum spectrum.⁴⁶ (In the present model calculation, the difference in the discreteness between the vibrational and the electronic states is imposed on the distinct spectral linewidths, i.e., the damping factors γ and Γ .)

For the nonzero $\delta\rho$ system, the symmetry-adapted modes Q_+ and Q_- should be mixed to form new eigenmodes. With the development of the mixing effect, the originally infrared-active mode, i.e., the Q_- mode for $\delta\rho = 0$, gains a Q_+ component along with $\delta\rho$. Since the e-mv coupling is mediated by the Q_- mode, its influence should be decreased with increasing $\delta\rho$. This tendency qualitatively explains the decrease in the band intensity of the fundamental mode and its frequency shift from the unperturbed position ($\sim 1450 \text{ cm}^{-1}$) with increasing $\delta\rho$ [Fig. 5(a)].

As shown in the figure, the spectra for nonzero $\delta\rho$ exhibited additional signals around ~ 2000 – 3000 cm^{-1} . Note that this band is positioned approximately at the twofold frequency of the fundamental vibrational signal in each spectrum, indicating that the additional structure is attributed to the overtone. The intensity of the structure varied with an increase of

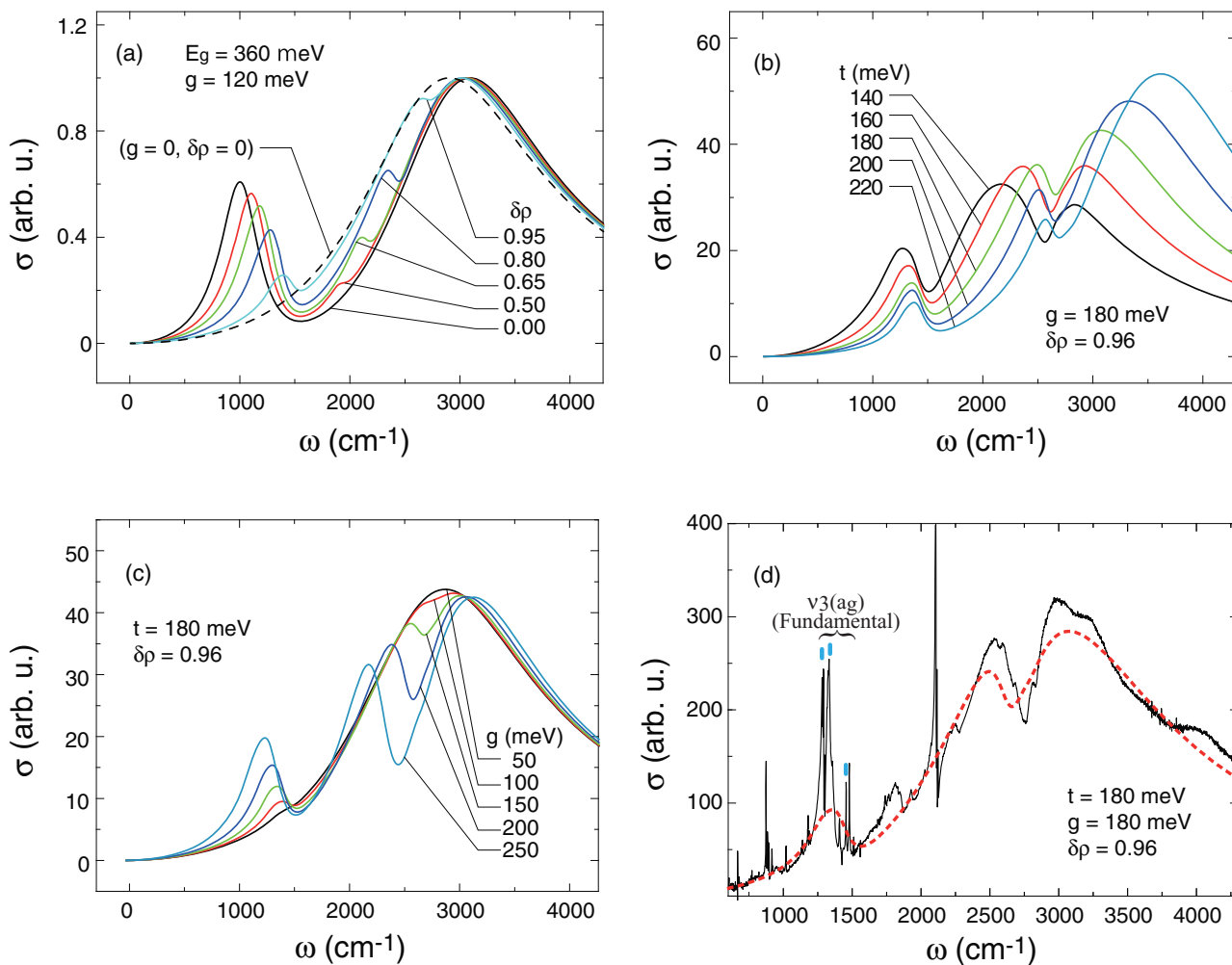


FIG. 5. (Color online) Optical conductivity spectra calculated using Eq. (4.19). (a), (b), and (c) show the $\delta\rho$, t , and g dependence of the spectra, respectively. The parameters used for the calculations are shown in each panel. (Common parameters: $\omega_{\text{neutral}} = 1494 \text{ cm}^{-1}$, $\omega_{\text{cation}} = 1407 \text{ cm}^{-1}$, $\Gamma = 100 \text{ cm}^{-1}$, and $\gamma = 1000 \text{ cm}^{-1}$.) The absolute value of the spectra in (a) has been normalized by the maximum conductivity of each data for the convenience of comparison. The dashed line in (a) shows the spectrum without vibronic coupling (see text). (d) Comparison of the calculated results (dotted line) to the experimentally obtained spectrum of θ -(BEDT-TTF)₂RbZn(SCN)₄ [E//a, $T = 6 \text{ K}$] (solid line). The sharp peaks marked with ticks are the fundamental signals of $\nu_3(a_g)$ [see Ref. 29].

$\delta\rho$; the band, which appeared at $\sim 2000 \text{ cm}^{-1}$ with nearly imperceptible intensity for $\delta\rho = 0.5$, grew into a sizable signal with increasing $\delta\rho$. The signal was then maximized around $\delta\rho \sim 0.85$, and finally diminished with a further increase of $\delta\rho$. Such $\delta\rho$ dependence agrees well with that of A_{CD} in Fig. 3(d).

It should be stressed that this signal is observable only for the system with a relatively large $\delta\rho$, indicating that the appearance of the overtone is viewed as an indication of large charge separation.

As mentioned above, the signal of the overtone is suggested to originate from the resonance between the vibrational levels and the charge-transfer band. Since the continuum state is not a completely flat spectrum but has a peak structure, the resonance depends largely on the mutual position of the signals for the discrete and the continuum states. Thus, the magnitude and the profile of the antiresonance structure vary with the frequency of the charge-transfer band as shown by the t dependence of the spectrum in Fig. 5(b). Furthermore, the overtone signal arises from the vibronic coupling of the Q_-

mode as the fundamental signal does, and hence the signal intensity is strongly dependent on the coupling constant. Figure 5(c) displays the g dependence of the overtone, which shows a significant increase with g , along with the fundamental signal appearing around $1000\text{--}1400 \text{ cm}^{-1}$. It should be noted that appreciable overtone signals may be observed when $g > 100 \text{ meV}$. As has been mentioned, the coupling constant for the ν_3 mode is estimated to be 132 meV . Thus, if the present calculation is quantitatively reliable, it is anticipated that a noticeable overtone signal would be observed when charge ordering occurs.

We have applied the numerical calculation to the simulation of the experimentally obtained spectrum of θ -(BEDT-TTF)₂RbZn(SCN)₄. It should be noted that this complex accommodates four BEDT-TTF molecules in the unit cell at low temperatures. According to Ref. 30, however, the BEDT-TTF molecules are tightly dimerized in the charge-ordered phase, thereby it is suggested that the essential spectroscopic feature may be governed by the electron

transitions within the dimeric unit. Such structural characteristics rationalize the application of the dimeric model for the simulation.

Figure 5(d) shows a comparison of the experimentally obtained spectrum of the complex $[\mathbf{E}/\mathbf{a}, T = 6 \text{ K}]$ and the result of the numerical calculation. Whereas the spectrum exhibited a number of vibrational signals over the broad electronic transition band, we focused only on the fundamental signals of the ν_3 mode (labeled by ticks) and the dip-shaped anomaly around 2700 cm^{-1} . In the numerical calculation we determined the transfer energy from the peak position of the charge-transfer band and subsequently tuned the two parameters $\delta\rho$ and g to reproduce the vibronic signals of the fundamental mode and the overtone of ν_3 .

The fundamental signals of ν_3 in the experimental spectrum are split into at least three bands due to the factor group splitting as marked by the ticks.²⁹ Although the present dimeric model cannot simulate the fine structure, the calculation reproduced the essential features of the experimental spectrum, i.e., frequency, intensity, and rough profile of the fundamental signal as well as the overtone. It should be emphasized that we have not assumed any fitting parameters peculiar to the overtone (we used only the frequency of the neutral and ionic states, the coupling constant, and the damping factor as the parameter for the fundamental mode of ν_3). In spite of the fact that limited numbers of parameters have been used, the calculation has reproduced the features of the spectrum, which in fact ascertains the validity of the theoretical arguments about the e-mv coupling properties in charge-ordered systems.

V. DISCUSSION

We have demonstrated that the dip anomaly appearing in the conductivity spectrum is attributed to the overtone of the C=C stretching mode. Since the signal becomes noticeable for large $\delta\rho$, the appearance of the overtone can be regarded as an indication that the system undergoes charge ordering, such as the Wigner crystallization of electrons.

As substances that show the charge ordering, two-dimensional organic compounds are establishing the representative position along with some metal oxides such as a series of magnetites⁴⁷ and NaV_2O_5 .^{48,49} Although there would be rich physical subjects associated with the correlation phenomenon, the number of studies on this phenomenon has been limited until recently. One reason for this may be attributed to the difficulty in identification of charge ordering. Unlike the charge-density-wave characteristic for one-dimensional systems, charge ordering generate significant charge disproportionation; in some compounds, molecules in the mixed-valency state are almost completely separated from the neutral and ionic species.⁵⁰ Even so, the amplitude of the electron inhomogeneity is very small in comparison to the total electron density, preventing clear identification of the charge ordering with structural analysis such as x-ray diffraction.

Vibrational spectroscopy may be an effective tool for this purpose, especially for organic compounds. This is because it offers us information on the molecular ionicity via the frequency of some vibrational modes. In fact, however, there is significant difficulty in the assignment of these signals, which

hinders the estimation of molecular charge. The difficulty in the assignment is associated with the fact that a number of vibrational modes coexist in the same frequency region where these modes appear. Furthermore, these signals can be largely shifted from the frequency determined by the molecular ionicity due to the e-mv coupling effect.

In contrast, the overtone signal studied here is easy to assign for the broad dip shape and the characteristic frequency. Therefore, the emergence of such a signal can be viewed as an indication of the occurrence of charge ordering. Moreover, we wish to stress an additional importance of the activation of the overtone. Emergence of appreciable overtone indicates a generation of significant anharmonicity in the electron-phonon system. For several materials, anharmonicity plays a crucial role for their unusual physical properties. In a recent example, anharmonic local phonons in a class of cage compounds are suggested to induce an enhanced thermoelectricity and superconductivity.⁵¹⁻⁵³ Hence, the appearance of the overtone would be noteworthy as a clue implying unusual physical properties.

We argued that the anharmonicity activating the overtone signal arises from the nonlinearity in the mixing of the electronic levels with respect to the Q_- value at equilibrium. As we have mentioned in Sec. IV A, the Q_- mode acts to the electronic system as if an electronic field does. This formal equivalence between the Q_- mode and the electric field suggests that the charge-ordered system showing the overtone signal may exhibit nonlinearities in the electronic properties when applied with strong electrical fields. To examine this idea, we have performed optical second-harmonic-generation measurements, which is a lowest-order nonlinear optical property. As widely known, the even-order nonlinear optical property can be observed for a crystal without inversion symmetry. We have selected α -(BEDT-TTF)₂I₃ [which is included in Fig. 1(c)] as the sample of the measurements because of a possible breakdown of the mutual exclusion rule for the Raman and the infrared spectra⁵⁴ and found that the complex shows large optical nonlinearity in the charge-ordered state.^{12,13}

In the present study, we have neglected the effects of electron correlations except for introducing the charge separation as the effective parameter. In reality, conduction electrons in strongly correlated systems are correlated with each other, which gives rise to various cooperating phenomena. Because of the cooperative nature of the electronic system, a local nonlinearity in the electronic transition might be amplified in the macroscopic system. So far, a number of studies have revealed that the charge-ordered or charge-fluctuating organic compounds show a range of nonlinear properties in dielectric and transport nature under strong fields. We suggest that these properties may have something to do with the nonlinear nature in the charge transfer of the charge-ordered systems argued in the present study.

VI. CONCLUSION

We studied the dip-shaped signal appearing in the optical conductivity spectrum of organic charge-transfer complexes in charge-ordered state. This signal was attributed to the overtone of the C=C stretching mode of molecular vibration by the

observation of isotope shift. With the help of the simple cluster model, we investigated the higher-order perturbation effects of the e-mv coupling phenomenon to the adiabatic potential of the cluster system when charge ordering occurs, and revealed that an anharmonicity was induced as the result of a higher-order vibronic correction of the electronic wave function in the symmetry broken system. We calculated the optical conductivity of the cluster system, and found that the dimeric model reproduced the features of the experimental spectrum, i.e., the shape and the frequency of the overtone and its fundamental band, illustrating the validity of the argument on the vibronic coupling effects in charge-ordered systems.

ACKNOWLEDGMENTS

We thank S. Iwai for continuing interest in our study. The ^{13}C -labeled sample of θ -(BEDT-TTF) $_2\text{RbZn}(\text{SCN})_4$ was supplied by A. Kawamoto, K. Miyagawa, and K. Kanoda. This work was partially supported by a Grant-in-Aid for Scientific Research on Innovative Areas (Grant No. 21110524), Scientific Research on Priority Areas of Molecular Conductors (Grant No. 15073211), Young Scientists (B) (Grant No. 17750139), and Exploratory Research (Grant No. 19655054), from the Ministry of Education, Culture, Sports, Science and Technology of Japan. One of the authors (A.K.) thanks the Japan Society for the Promotion of Science (ID No. P 06359) for financial support.

APPENDIX

The symmetric coordinates Q_+ and Q_- are not the valid eigenmodes of a charge-separated system. The force constant (Hessian) matrix $F(Q_+, Q_-)$ of the charge-separated system is defined as

$$F(Q_+, Q_-) = \begin{pmatrix} \frac{\partial^2 H}{\partial Q_+^2} & \frac{\partial^2 H}{\partial Q_+ \partial Q_-} \\ \frac{\partial^2 H}{\partial Q_- \partial Q_+} & \frac{\partial^2 H}{\partial Q_-^2} \end{pmatrix} = \frac{1}{2} \begin{pmatrix} \omega_{\text{avg}} & g^{(2)} \delta \rho \\ g^{(2)} \delta \rho & \omega_{\text{avg}} - \frac{2g^2 \delta n_{\text{eg}}^2}{E_{\text{eg}}} \end{pmatrix}, \quad (\text{A1})$$

where H denotes the total Hamiltonian of the system and $\omega_{\text{avg}} = (1/2)(\omega_{\text{cation}} + \omega_{\text{neutral}})$.

The new normal modes (named as R and S) [and thus the respective eigenfrequencies (ω_R, ω_S) as well] should be obtained from the diagonalization of the matrix as the form of the linear combination of Q_+ and Q_- , i.e.,

$$\begin{pmatrix} R \\ S \end{pmatrix} = \mathbf{A} \begin{pmatrix} Q_+ \\ Q_- \end{pmatrix}. \quad (\text{A2})$$

The coefficients ζ and ξ appearing in Sec. IV A are determined from the inversion of the coefficient matrix, i.e.,

$$\begin{pmatrix} \xi & -\zeta \\ \zeta & \xi \end{pmatrix} = \mathbf{A}^{-1}, \quad (\text{A3})$$

where $\xi^2 + \zeta^2 = 1$.

*yamamoto@ims.ac.jp.

¹K. Hiraki and K. Kanoda, *Phys. Rev. Lett.* **80**, 4737 (1998).

²H. Seo, C. Hotta, and H. Fukuyama, *Chem. Rev.* **104**, 5005 (2004).

³F. Sawano, I. Terasaki, H. Mori, T. Mori, M. Watanabe, N. Ikeda, Y. Nogami, and Y. Noda, *Nature (London)* **437**, 522 (2005).

⁴T. Mori, Y. Bando, T. Kawamoto, I. Terasaki, K. Takimiya and T. Otsubo, *Phys. Rev. Lett.* **100**, 037001 (2008).

⁵Y. Takahide, M. Kimata, K. Hazama, T. Terashima, S. Uji, T. Konoike, and H. M. Yamamoto, *Phys. Rev. B* **81**, 235110 (2010).

⁶F. Nad, P. Monceau, and H. M. Yamamoto, *J. Phys.: Condens. Matter* **20**, 485211 (2008).

⁷N. Tajima, J. Fujisawa, N. Naka, T. Ishihara, R. Kato, Y. Nishio, and K. Kajita, *J. Phys. Soc. Jpn.* **74**, 511 (2005).

⁸M. Chollet, L. Guerien, N. Uchida, S. Fukaya, H. Shimoda, T. Ishikawa, K. Matsuda, T. Hasegawa, A. Ota, H. Yamochi, G. Saito, R. Tazaki, A. Adachi, and S. Koshihara, *Science* **307**, 86 (2005).

⁹S. Iwai, K. Yamamoto, A. Kashiwazaki, F. Hiramatsu, H. Nakaya, Y. Kawakami, K. Yakushi, H. Okamoto, H. Mori, and Y. Nishio, *Phys. Rev. Lett.* **98**, 097402 (2007).

¹⁰T. Ishikawa, N. Fukazawa, Y. Matsubara, R. Nakajima, K. Onda, Y. Okimoto, S. Koshihara, M. Lorenc, E. Collet, M. Tamura, and R. Kato, *Phys. Rev. B* **80**, 115108 (2009).

¹¹P. Monceau, F. Y. Nad, and S. Brazovskii, *Phys. Rev. Lett.* **86**, 4080 (2001).

¹²K. Yamamoto, S. Iwai, S. Boyko, A. Kashiwazaki, F. Hiramatsu, C. Okabe, N. Nishi, and K. Yakushi, *J. Phys. Soc. Jpn.* **77**, 074709 (2008).

¹³K. Yamamoto, A. A. Kowalska, and K. Yakushi, *Appl. Phys. Lett.* **96**, 122901 (2010).

¹⁴S. Mazumdar, R. T. Clay, and D. K. Campbell, *Phys. Rev. B* **62**, 13400 (2000).

¹⁵J. Merino and R. H. McKenzie, *Phys. Rev. Lett.* **87**, 237002 (2001).

¹⁶M. Dressel, N. Drichko, J. Schlueter, and J. Merino, *Phys. Rev. Lett.* **90**, 167002 (2003).

¹⁷K. Kuroki, *J. Phys. Soc. Jpn.* **75**, 114716 (2006).

¹⁸H. Watanabe and M. Ogata, *J. Phys. Soc. Jpn.* **75**, 063702 (2006).

¹⁹S. Kimura, H. Suzuki, T. Maejima, H. Mori, J. Yamaura, T. Kak-iuchi, H. Sawa, and H. Moriyama, *J. Am. Chem. Soc.* **128**, 1456 (2006).

²⁰R. Kondo, M. Higa, S. Kagoshima, N. Hanasaki, Y. Nogami, and H. Nishikawa, *Phys. Rev. B* **81**, 024519 (2010).

²¹N. O. Lipari, C. B. Duke, and L. Pietronero, *J. Chem. Phys.* **65**, 1165 (1976).

²²M. J. Rice, *Solid State Commun.* **31**, 93 (1979).

²³R. Bozio, M. Meneghetti, and C. Pecile, *Phys. Rev. B* **36**, 7795 (1987).

²⁴A. Painelli and A. Girlando, *J. Chem. Phys.* **84**, 5655 (1986).

²⁵V. M. Yartsev and R. Swietlik, *Reviews of Solid State Science* (World Scientific, Singapore, 1990), Vol. 4, p. 247.

²⁶H. Mori, S. Tanaka, and T. Mori, *Phys. Rev. B* **57**, 12023 (1998).

²⁷K. Miyagawa, A. Kawamoto, and K. Kanoda, *Phys. Rev. B* **62**, R7679 (2000).

²⁸R. Chiba, H. M. Yamamoto, K. Hiraki, T. Nakamura, and T. Takahashi, *Synth. Met.* **120**, 919 (2001).

²⁹K. Yamamoto, K. Yakushi, K. Miyagawa, K. Kanoda, and A. Kawamoto, *Phys. Rev. B* **65**, 085110 (2002).

- ³⁰M. Watanabe, Y. Noda, Y. Nogami, and H. Mori, *J. Phys. Soc. Jpn* **73**, 921 (2004).
- ³¹S. Miyashita and K. Yonemitsu, *Phys. Rev. B* **75**, 245112 (2007).
- ³²Y. Tanaka and K. Yonemitsu, *J. Phys. Soc. Jpn.* **76**, 053708 (2007).
- ³³H. Tajima, S. Kyoden, H. Mori, and S. Tanaka, *Phys. Rev. B* **62**, 9378 (2000).
- ³⁴M. Mori and K. Yonemitsu, *J. Phys. Chem. Solid* **62**, 409 (2001).
- ³⁵Y. Ding and H. Tajima, *Phys. Rev. B* **69**, 115121 (2004).
- ³⁶K. Suzuki, K. Yamamoto, and K. Yakushi, *Phys. Rev. B* **69**, 085114 (2004).
- ³⁷J. Ouyang, K. Yakushi, Y. Misaki, and K. Tanaka, *Phys. Rev. B* **63**, 054301 (2001).
- ³⁸M. Uruichi, K. Yakushi, H. M. Yamamoto, and R. Kato, *J. Phys. Soc. Jpn.* **75**, 074720 (2006).
- ³⁹M. E. Kozlov, K. I. Pokhodnia, and A. A. Yurchenko, *Spectrochim. Acta, Part A* **45**, 437 (1989).
- ⁴⁰J. C. Faulhaber, D. Y. Ko, and P. R. Briddon, *Synth. Met.* **60**, 227 (1993).
- ⁴¹G. Visentini, M. Masino, C. Bellitto, and A. Girlando, *Phys. Rev. B* **58**, 9460 (1998).
- ⁴²K. Shizu, T. Sato, and K. Tanaka, *Chem. Phys. Lett.* **491**, 65 (2010).
- ⁴³M. E. Kozlov, K. I. Pokhodnia, and A. A. Yurchenko, *Spectrochim. Acta, Part A* **43**, 323 (1987).
- ⁴⁴H. H. Wang, R. Ferraro, J. M. Williams, U. Geiser, and A. Schlueter, *J. Chem. Soc. Chem. Commun.* 1893 (1994).
- ⁴⁵T. Yamamoto, M. Uruichi, K. Yamamoto, K. Yakushi, A. Kawamoto, and H. Taniguchi, *J. Phys. Chem. B* **109**, 15226 (2005).
- ⁴⁶U. Fano, *Phys. Rev.* **124**, 1866 (1961).
- ⁴⁷F. Walz, *J. Phys.: Condens. Matter.* **14**, R285 (2002).
- ⁴⁸H. Seo and H. Fukuyama, *J. Phys. Soc. Jpn.* **67**, 2602 (1998).
- ⁴⁹P. Thalmeier and P. Fulde, *Europhys. Lett.* **44**, 242 (1998).
- ⁵⁰Y. Yue, C. Nakano, K. Yamamoto, M. Uruichi, R. Wojciechowski, M. Inokuchi, K. Yakushi, and A. Kawamoto, *J. Phys. Soc. Jpn.* **78**, 044701 (2009).
- ⁵¹V. Keppens, D. Mandrus, B. C. Sales, B. C. Chakoumakos, P. Dai, R. Coldea, M. B. Maple, D. A. Gajewski, E. J. Freeman, and S. Bennington, *Nature (London)* **395**, 876 (1998).
- ⁵²G. S. Nolas, J. L. Cohn, G. A. Slack, and S. B. Schujman, *Appl. Phys. Lett.* **73**, 178 (1998).
- ⁵³Y. Nagao, J. Yamaura, H. Ogusu, Y. Okamoto, and Z. Hiroi, *J. Phys. Soc. Jpn.* **78**, 064702 (2009).
- ⁵⁴R. Wojciechowski, K. Yamamoto, K. Yakushi, M. Inokuchi, and A. Kawamoto, *Phys. Rev. B* **67**, 224105 (2003).